European Journal of Pharmaceutics and Biopharmaceutics 77 (2011) 368–375

Contents lists available at ScienceDirect

European Journal of Pharmaceutics and Biopharmaceutics

journal homepage: www.elsevier.com/locate/ejpb

Research paper

Cerium oxide nanoparticle uptake kinetics from the gas-phase into lung cells *in vitro* is transport limited

David O. Raemy [a,*], Ludwig K. Limbach [b], Barbara Rothen-Rutishauser [a], Robert N. Grass [b], Peter Gehr [a], Karin Birbaum [c], Christina Brandenberger [a], Detlef Günther [c], Wendelin J. Stark [b]

[a] *Institute of Anatomy, Division of Histology, University of Bern, Bern, Switzerland*
[b] *Functional Materials Laboratory, D-CHAB, ETH Zurich, Zurich, Switzerland*
[c] *Laboratory of Inorganic Chemistry, D-CHAB, ETH Zurich, Zurich, Switzerland*

ARTICLE INFO

Article history:
Available online 28 November 2010

Keywords:
Nanoparticle
Lung cell cultures
Uptake kinetics
Air–liquid interface
Cerium oxide

ABSTRACT

Nowadays, aerosol processes are widely used for the manufacture of nanoparticles (NPs), creating an increased occupational exposure risk of workers, laboratory personnel and scientists to airborne particles. There is evidence that possible adverse effects are linked with the accumulation of NPs in target cells, pointing out the importance of understanding the kinetics of particle internalization.

In this context, the uptake kinetics of representative airborne NPs over 30 min and their internalization after 24 h post-exposure were investigated by the use of a recently established exposure system. This system combines the production of aerosolized cerium oxide (CeO_2) NPs by flame spray synthesis with its simultaneous particle deposition from the gas-phase onto A549 lung cells, cultivated at the air–liquid interface.

Particle uptake was quantified by mass spectrometry after several exposure times (0, 5, 10, 20 and 30 min). Over 35% of the deposited mass was found internalized after 10 min exposure, a value that increased to 60% after 30 min exposure. Following an additional 24 h post-incubation, a time span, after which adverse biological effects were observed in previous experiments, over 80% of total CeO_2 could be detected intracellularly.

On the ultrastructural level, focal cerium aggregates were present on the apical surface of A549 cells and could also be localized intracellularly in vesicular structures. The uptake behaviour of aerosolized CeO_2 is in line with observations on cerium suspensions, where particle mass transport was identified as the rate-limiting factor for NP internalization.

1. Introduction

Gas-phase processes are routinely used for manufacturing commercial quantities of a wide range of nanoparticles (NPs) such as pigments, heterogeneous catalysts, and reinforcing and polishing agents. Typical commodities are carbon black and ceramic powders like pigmentary titania and fumed silica, products that have already been on the market for many decades with annual production volumes of several megatons [1–3]. The production of sub-micron particles in gas-phase reactors is associated with a potential release of aerosolized primary particles or particle aggregates into the working environment during the synthesis stage, powder recovery and in any further processing or packing [4]. The versatility, broad applicability and inexpensiveness of this technology makes it attractive for the production of materials on an industrial and laboratory scale, creating an increased (chronic or acute) potential risk of exposure for workers, laboratory personnel and scientists to aerosols in occupational settings [2].

There is epidemiological evidence for adverse health effects caused from inhaled NPs [5], although the underlying generic toxicity mechanisms and particle toxicokinetics are not completely understood so far. The classical dose–response paradigm links possible adverse effects with NP – dose in target cells. This points out the importance of understanding the kinetic aspect of particle uptake. *In vitro* kinetic studies have been performed, for example with quantum dots [6,7], polymeric nanoparticles [8,9] such as

Abbreviations: NP, nanoparticle; CeO_2, cerium oxide; ICP-MS, inductively coupled plasma mass spectrometry; LDH, lactate dehydrogenase; TEM, transmission electron microscope; OsO_4, osmium tetroxide; XRD, X-ray powder diffraction; XDC, X-ray disc centrifugation; SSA, specific surface area; d_{BET}, Brunauer–Emmett–Teller (BET)-equivalent particle diameter; OD, optical density; d, day; ESI, electron spectroscopic imaging; M, mass.

* Corresponding author. Institute of Anatomy, Division of Histology, University of Bern, Baltzerstrasse 2, CH-3000 Bern 9, Switzerland. Tel.: +41 (0) 31 631 46 09.
E-mail address: raemy@ana.unibe.ch (D.O. Raemy).

0939-6411/$ - see front matter © 2010 Elsevier B.V. All rights reserved.
doi:10.1016/j.ejpb.2010.11.017

albumin coated polylactic polyglycolic acid co-polymers [10–12], gold NPs [13–16], d(GT)$_{15}$ wrapped single walled carbon nanotubes [17], chromium nanoparticles [18], anionic superparamagnetic iron oxide [19,20] and cerium oxide NPs [21].

To date, our knowledge on particle penetration through the cellular membrane, as a biological barrier, is based on investigations carried out in submerged cell cultures which have been exposed to particle suspensions, which is the generic methodological background of all the above-mentioned studies. In contrast, there is not much knowledge on the uptake kinetics of aerosol particles into air–liquid cultivated cell cultures, exposed to NPs from the gas-phase, the realistic exposure scenario for airborne particle types. This more physiological approach has been used so far to investigate the effects of various particle types important for human health [22,23] and considers the influence of the physicochemical environment (air instead of culture medium) on biological responses [24,25].

Under air–liquid conditions, the lung cells are separated from the air only by a thin aqueous lining layer with a surfactant film at the air–liquid interface [26,27], onto which particles are deposited. At these defined extracellular surface structures, interfacial phenomena (e.g. surface tension leading to wetting and displacement of NPs) take place [26,28–30], making the physics of particle translocation more realistic compared to conventional submersed cultures.

To elucidate the *in vitro* uptake kinetics of a representative aerosolized NP, flame-made cerium oxide (CeO_2) was been chosen for this study. This insoluble metal oxide is in wide use in industrial settings as for example as catalyst, polishing compound, glass manufacturing additive and pigment [31,32]. Beside its occupational relevance, CeO_2 is also an emerging environmental factor, because of its use as a fuel additive [33–37]. The intracellular localization has already been demonstrated in different cell cultures by the use of microscopy [21,36,38,39]. Furthermore, lung persistent, elemental cerium-containing particles were described in a few clinical case studies [40–44] related to the pathology of rare earth pneumoconiosis. The analytical advantage of being easily detectable by inductively coupled plasma mass spectroscopy (ICP-MS), with no interference with the cell cultures biological element content [21,45], makes this particle type an adequate tool for fundamental mechanistic studies.

Limbach et al. [21] measured uptake kinetics of CeO_2 into a human lung fibroblast cell line, which was exposed to particle suspensions of four different size classes, covering a range of 20–500 nm. Physical NP transport processes to the medium-exposed cellular interfacial surface, either by sedimentation (size fraction 250–500 nm) or diffusion (size fraction 25–50 nm), were identified as rate-limiting factors for particle uptake kinetics by applying a mathematical model using only measurable parameters. From this, it follows that under these conditions, particle uptake by the cells can be assumed to be a much faster process than the directed physical mass transport to the cellular surface. A linear accumulation over the first 4 h was observed for administered low, physiologically relevant cerium concentrations of 100 ng up to 1 μg g^{-1} culture medium, uptake kinetics also found for chromium NPs over a comparable time range [18]. Such a fast, approximate linear, initial particle uptake seems to represent the initial phase of the saturation curve, describing the generic NP uptake kinetics over more prolonged time spans, as consistently reported in the literature [6–17,19,20].

Although particle dispersions in liquid (suspension) and such in gas (aerosol) behave according to the same physicochemical principals, mass transport by diffusion and sedimentation can be considered as much faster process in the gas-phase. We therefore hypothesize a transport limitation of particle uptake kinetics also in an aerosol exposure scenario. To test this assumption, monocultures of the A549 cell line [46] were exposed to airborne CeO_2 with a novel exposure system, recently established and characterized by Rothen-Rutishauser et al. [22]. This approach combines the production of a dry, dispersion-medium free, NP aerosol in a closed air–volume by an industrially used flame process, with the simultaneous passive particle deposition from the gas-phase on the surface of lung cell cultures. By using this system, the total mass deposition as well as the intracellular cerium mass could be determined over time for assessing the uptake kinetics of this particle type.

2. Materials and methods

2.1. Nanoparticle production

An aerosol exposure system, recently implemented by Rothen-Rutishauser et al. was used to deposit airborne CeO_2 particles onto A549 cell cultures at the air–liquid interface [22]. The exposure system was installed in a gas-tight glove-box apparatus with a continuously mixed inner volume of 2.5 m^3. A cerium oxide particle aerosol was prepared by flame spray synthesis, using cerium (8 wt.%) dissolved in 2-ethylhexanoic acid diluted in xylene as precursor [21]. The precursor was fed through a capillary with a diameter of 0.4 mm into a methane–oxygen supporting flame at a rate of 5 mL min^{-1}. Liquid leaving the capillary was dispersed in oxygen (5 L min^{-1}, 99.8%, Pan Gas, Dagmersellen, Switzerland), resulting in a burning spray of about 10 cm in height [47]. For the here reported experiments, the reactor was operated for 90 s.

2.2. Cell cultures

Cell cultures were prepared as described elsewhere [22]. Briefly, the A549 cell line representing alveolar type-II cells was obtained from the American Tissue Type Culture Collection (LGC Promochem, Molsheim, France). Cells were maintained in RPMI 1640 medium (containing 25 mM HEPES, Invitrogen, Basel, Switzerland) supplemented with 1% (v/v) L-Glutamine (LabForce AG, Nunningen, Switzerland), 1% (v/v) penicillin/streptomycin (Gibco BRL, Life Technologies, Basel, Switzerland), and 10% (v/v) fetal bovine serum (LabForce AG, Nunningen, Switzerland). Cells were seeded on BD Falcon™ cell culture inserts (High pore density PET membranes for 6-well plates with a growth area of 4.2 cm^2 and 3.0 μm pores; Becton Dickinson, Allschwil, Switzerland). Inserts were placed in 6-well BD Falcon™ tissue culture plates (Becton Dickinson, Allschwil, Switzerland) with 2 mL medium in the upper and 3 mL in the lower chamber. Cells were grown to confluence under immersed conditions for 7 days. Afterwards, the medium in the upper chamber was removed completely, while the medium volume in the lower chamber was reduced to 1.2 mL. The cells were then exposed to air for 24 h to allow secretion of surfactant [48] and subsequently exposed to CeO_2 in the glove-box apparatus.

2.3. Exposure experiments

The aerosolized particles were directly deposited from the gas-phase onto A549 cell cultures over various timespans (0–30 min). Samples were prepared for mass spectrometry either after a washing step to remove adherent cerium (kinetics study) or without washing for the determination of total mass deposition per culture. After an additional 24 h post-incubation time, a second sample set was prepared for mass spectrometry and additionally analyzed by microscopic imaging. Further atmospheric parameters such as temperature and relative humidity were measured with a commercial digital thermo-hygrometer.

2.4. Flame off-gas control

Cultures exposed to flame off-gases only (reactor runtime 90 s) for 30 min served as cerium-free controls (“gas control”) and cells placed in an incubator during the exposure time (30 min) were used as “external controls” to assess the influence of handling and experimental setup on the culture behaviour.

2.5. Lactate dehydrogenase assay

Cell death was ascertained by measuring the release of lactate dehydrogenase (LDH) from necrotic cells. For that purpose, the medium of the lower well was collected in samples that were 24 h post-incubated after particle exposure. The supernatants were analyzed using the commercial colorimetric LDH cytotoxicity detection kitPLUS (Roche Applied Science, Mannheim, Germany) according to the supplier’s manual. Each supernatant was measured in triplicate. The values were expressed as $OD_{490\ nm-630\ nm}$ against a cell lysate as a positive control (2% Triton X-100 detergents for 30 min). The potential for the LDH enzyme to adsorb to the particle surface, and therefore result in a false-negative toxicity was assessed previously [22].

2.6. Transmission electron microscopy

For electron optical particle localization, cell cultures were fixed in 2.5% glutaraldehyde in 0.03 M potassium phosphate buffer. To analyze cell morphology with a focus on preserving fragile structures such as surfactant and the aqueous lining layer, the cells were first immersed in 1% OsO_4 in FC-72 (3M, Rüschlikon, Switzerland) for 7 min at room temperature, washed three times in FC-72 fluorocarbon and fixed in glutaraldehyde. The specimens were then further processed as described below [49]. After washing with potassium phosphate buffer, post-fixation with 1% osmium tetroxide in sodium cacodylate buffer and further washing with maleate buffer, the samples were stained with 0.5% uranyl acetate in maleate buffer. The cells were dehydrated in an ascending ethanol series and embedded in Epon. Ultrathin sections were cut, mounted on coated single slot copper grids and post-stained with uranyl acetate and lead citrate if required for increased contrast. Conventional imaging was done with a Morgagni TEM at 80 kV (FEI, Eindhoven, The Netherlands).

Elemental microanalysis was performed by cerium-specific electron spectroscopic imaging (ESI) with a Tecnai F20 TEM (FEI, Eindhoven, The Netherlands), operated at 200 kV and equipped with a GIF Tridiem energy filter and an Ultrascan 1000 CCD camera (Gatan, Pleasanton, USA). ESI images were taken following Brandenberger et al. [50]. Cerium energy loss images were recorded according to a three-window approach, including one post-edge (125 eV) and two pre-edge images (pre-edge 1 of 90 eV and pre-edge 2 of 100 eV). The slit width was set to 10 eV, exposure time was 4 s, with an image binning of 1 and a readout image average of four images per exposure.

To analyze cerium oxide deposition, coated single slot copper grids, placed in cell culture inserts located in 6-well plates, were directly exposed to the particle aerosol. Samples were analyzed without any further processing.

2.7. Particle characterization

NPs were collected for further characterization on a glass fiber filter (GF/A, 25.7 cm diameter, Whatmann, Bottmingen, Switzerland), placed on a cylinder mounted above the flame, by the aid of a vacuum pump (Seco SV 1040 C, Busch, Magden, Switzerland). The resulting nanopowder was sieved using 450 μm mesh. Its specific surface area (SSA) was measured on a Tristar (Micromeritics, Aachen, Germany) instrument by nitrogen adsorption at 77 K using the Brunauer–Emmett–Teller (BET) method with samples outgassed at 150 °C for 1 h prior to three analyses. The average BET-equivalent particle diameter d_{BET} was calculated using $d_{BET} = 6/(SSA \cdot \rho)$, where ρ denotes the density (kg m^{-3}) [51]. A powder diffraction (XRD) pattern was collected on a X’Pert PRO-MPD (X’Celerator linear detector system, PANalytical, Zurich, Switzerland, CuK_α radiation, step size of 0.033°, ambient conditions) to confirm the identity and crystallinity of the material.

Full particle size analyses were measured by X-ray disc centrifugation (XDC, Brookhaven Instruments Corporation, Holtsville, USA). Prior to measurements particles were dispersed in ultrapure water (resistivity > 18.2 MΩ cm^{-1}, Millipore, Zug, Switzerland) and stabilized with Dispex A40 (Ciba Specialty Chemicals, BASF Fine Chemicals, Evionnaz, Switzerland). After 5 min of sonication (UP-400S, Hielscher Ultrasonics, Teltow, Germany), the hydrodynamic particle diameter was measured on an X-ray disc centrifuge [21].

It is referred to Ref. [52] for further information on the general limitations of the analytical methods, used for particle characterization.

A Pyrochrome Limulus Amebocyte Lysate endotoxin test (Pyroquant Diagnostik, Mörfelden, Germany) of the nanopowder was performed according to the supplier’s manual. Pictures were taken with a Canon EOS 20D with a macro lens.

2.8. Cerium element analysis by inductively coupled plasma mass spectrometry (ICP-MS)

The analysis procedure was carried out according to Limbach et al. [21]. Briefly, cerium-exposed cultures dedicated to determine “internal dose” (intracellular and tightly associated CeO_2) were washed three times with 1 mL isotonic 0.9% NaCl (upper and lower well) to remove non-adherent or slightly adsorbed CeO_2 and the used washing solution was saved for further control experiments. “Total deposition” per culture insert was measured in exposed cell cultures, which were analyzed directly by mass spectrometry without any washing procedure (sum of intracellular and extracellular fraction).

Then, membranes were dried at room temperature and transferred into pre-cleaned digestion vials by consecutive dissolution in 1 mL and 0.5 mL sub-boiled nitric acid (65%, p.a., Merck, Darmstadt, Germany; sub-boiled with a, Duopor Acid Purification System, Milstone MLS, Sorisole, Italy) per well for 30 min. A total of 200 μL H_2O_2 (30%, trace select ultra, Fluka Analytical, Sigma–Aldrich Chemie, Buchs, Switzerland) and 100 ng g^{-1} yttrium (Y) were added followed by sonication for 10 min (RK510, Bandelin Electronics, Berlin, Germany). Samples were digested (Ultra Clave II digestion unit, Milestone MLS, Sorisole, Italy) by increasing the temperature and pressure to 230 °C/90 bars over 75 min. Then, samples were diluted using ultrapure water (Millipore, Zug, Switzerland) to 10 g total weight. Specimens were further diluted by a factor of 10 and 10 ng g^{-1} Indium (In) was added as internal standard. Cerium concentrations were measured using an external calibration on an inductively coupled plasma sector field mass spectrometer (Element 2 ICP-MS, Thermo Scientific, Bremen, Germany). Ce, In and Y standards were diluted from certified single element standards (1000 μg g^{-1}, Merck, Darmstadt, Germany).

2.9. Control experiments

To assess the cerium-specific analytical quality of the applied ICP-MS procedure, a mass (M) balance was calculated ($M_{cell\ associated} + M_{washing\ solution} = M_{total\ deposited}$) for 30 min exposed culture inserts, measured either directly after exposure or after an additional 24 h post-incubation.

Several air–liquid cultures of A549 were washed using the same procedure as used for the preparation of ICP-MS samples, followed by OsO_4 fixation for TEM (see above). The presence and morphology of the thereby preserved lipid rich cell-associated structures, as the surfactant layer and the underlying aqueous hypophase, were analyzed microscopically to assess the efficiency of the applied washing protocol.

Furthermore, cultures grown for 1 and 2 days at the air–liquid interface were assessed for cell loss, caused by the mechanical conditions of the MS-washing procedure by comparing the cell number of unwashed and washed cultures. For that purpose, unwashed controls or washed cultures were fixed with 3% paraformaldehyde in PBS for 15 min at room temperature, followed by subsequent storage in 0.1 M glycine (in PBS). Then, samples were permeabilized by 0.2% Triton X-100 (in PBS), washed in PBS (RT) and stained by DAPI (1:100) for 1 h at RT to visualize the cell nuclei. Specimens were washed tree times in PBS, mounted in Mowiol (Carl Roth, Karlsruhe, Germany) and stored at 4 °C until analysis by Laser Scanning Microscopy (LSM510 Meta, Carl Zeiss, Feldbach, Switzerland). The DAPI channel was superimposed by an unbiased stereological counting frame of a defined area, and the number of nuclei per area density was extrapolated to the 4.2 cm^2 surface area of a culture well as reference space.

2.10. Statistics

Values were expressed as mean ± standard deviation (SD). Statistical analysis was performed with SPSS 14.0 (SPSS Schweiz AG, Zürich, Switzerland). A Wilcoxon rank-sum test was applied and values considered as significant at $p < 0.05$.

3. Results

3.1. Particle characterization

The specific surface area of flame-made CeO_2 NPs, produced under the same conditions as in the exposure system, was determined as 88 m^2 g^{-1}, resulting in an average BET-equivalent particle diameter of 8.9 nm. Chemical identity, purity and crystallinity of the nanopowder were confirmed by XRD powder diffraction (Fig. S1 A). Additionally, the hydrodynamic particle size distribution in an aqueous suspension was measured by XDC (mean diameter: 24 nm, geometric standard deviation: 1.45) (Fig. S1 B). Cerium oxide appears macroscopically as pale, yellow-white powder (Fig. S1 C) and was analyzed to be endotoxin-free (data not shown).

3.2. Characteristics of deposited particles

The CeO_2 deposition was characterized by exposing TEM grids on the bottom of the chamber to the produced aerosol. The airborne particles agglomerated very fast, which is in good agreement with theoretical calculations. Fig. 1A shows the cumulative cerium NP deposition over 10 min after particle production. CeO_2 NPs get in contact with the cell cultures as fractal agglomerates of various sizes. The chemical nature and purity of the deposited matter was confirmed by cerium-specific electron spectroscopic imaging (ESI) of multiple randomly selected aggregates (Fig. 1B) consisting of primary particles with a cubic lattice (Fig. 1C). Furthermore, a homogenous mass deposition over the entire experimental setup was demonstrated by analyzing TEM grids, placed at different positions at the bottom of the aerosol chamber (Fig. 1D).

3.3. Particle visualization in biological samples

Agglomeration in the glove-box atmosphere causes a sedimentation-driven mass deposition, as already demonstrated (see above). The A549 cells became in contact with the cerium NPs in an agglomerated state. The electron microscopic investigation of exposed cell cultures revealed focal cerium agglomerates (lateral dimensions of a few nanometers (Fig. 2A) up to microns (Fig. 2B)) on the cellular apical surface with no obvious local preference of adsorption. These membrane associated aggregates followed the cell's surface morphology very closely

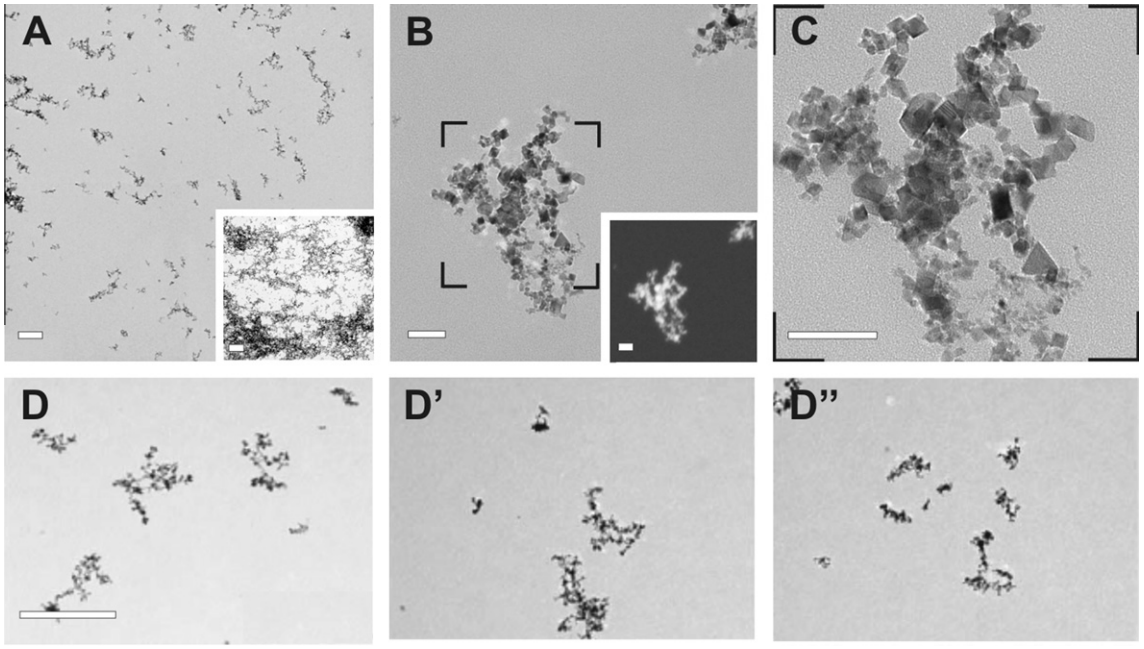

Fig. 1. Analysis of CeO_2 deposition onto TEM grids, which have been placed inside the glove box. (A) Cumulative deposition over 10 and 60 min (inset). (B) Electron spectroscopic imaging (ESI) cerium element analysis (inset) of an aggregate. (C) Magnified area indicated on micrograph B: the Nanoceria primary particles appear as sharp-edged crystals with a cubic lattice. (D–D″.) TEM grids placed at different positions in the exposure chamber illustrate a homogenous mass deposition per area over the entire experimental setup. Scale bars: A/D 500 nm, B/C 50 nm.

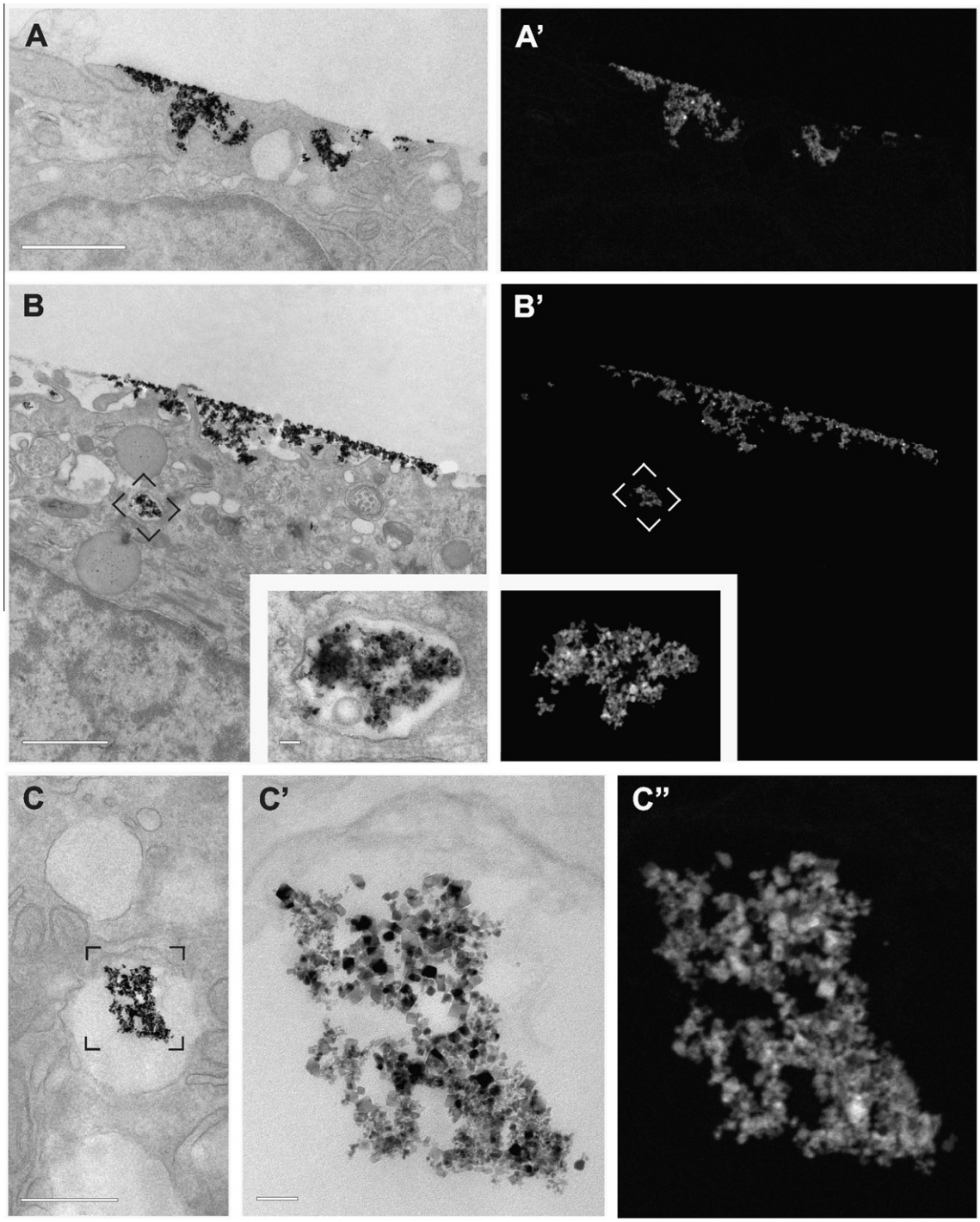

Fig. 2. Particle localization and *in situ* ESI element analysis of cerium oxide. (A) Electron micrograph of an A549 monoculture, exposed for 10 min to aerosolized CeO_2. Electron dense structures in the sub-micron range are decorating the apical plasma membrane. (A′) The corresponding ESI element analysis of the same field identifies these structures as cerium. (B) Exposure to cerium oxide for 30 min. CeO_2 is found to be associated with the apical membrane as flattened agglomerate (lateral dimension in the micrometer range) and is localized intracellularly in vesicles (see inset). To increase contrast, the sample was post-stained with uranyl acetate and lead citrate. (B′) Corresponding ESI element analysis. (C) A cerium oxide agglomerate found inside a vesicle of a 30-min exposed culture. (C′) Magnification of C. with a corresponding ESI analysis shown in C″. Scale bars: A/C 500 nm, B 1 μm, B insets and C′/C″ 50 nm.

and seemed to be localized in the aqueous hypophase underneath the surfactant film, although these structures were not preserved completely by the technique used. Furthermore, cerium oxide was found to invade deeply into the intercellular space (Fig. S2 A). Intracellular CeO_2 aggregates were observed in vesicular structures in 10 min and also 30 min exposed cell cultures (Fig. 2B/C), whereby the internalized agglomerates reached sizes up to the micrometer (Fig. S2 B). High-resolution micrographs demonstrated *in situ* the characteristic crystalline structure of cerium primary particles, which was additionally confirmed by ESI microanalysis (Fig. 2B inset/C). For some intracellular agglomerates, no surrounding membrane could be found and the structures appeared as to float free by in the cytoplasm (Fig. S2 C).

3.4. CeO_2 uptake kinetics in A549 monocultures

Monocultures of the cultivated A549 lung epithelial cells at the air–liquid interface were exposed for 5, 10, 20 and 30 min to a flame-made CeO_2 particle aerosol (Fig. 3). Three different measurements were preformed; the total deposited mass per cell culture well, the amount of cellular internalized cerium oxide directly after exposure as well as after a 24 h post-incubation. Data were expressed in a "Mass per culture" dose-metrics, as recently suggested by Teeguarden et al. [53].

The total deposited mass per well (insert area = 4.2 cm^2) was determined to be 1.5 (SD 0.4), 5.3 (SD 0.1) and 7.8 (SD 0.1) μg, after 10, 20 and 30 min ($n = 2$), respectively. This increase is associated with the reduction of CeO_2 in the chamber atmosphere over this time span.

The mean cerium uptake immediately after exposure was 0.2 (SD 0.1), 0.5 (SD 0.3), 2.4 (SD 0.8), 4.6 (SD 1.4) μg $well^{-1}$, after 5, 10, 20 and 30 min exposure time ($n = 2$). After 10-min exposure, over 35% of the total deposited cerium mass remained intracellular after surface washing, a value that increased to 60% after 30-min exposure. The uptake mechanism was not saturated over the investigated time span, internalization is in general very fast and approximately linear, as previously observed for nanoparticle suspensions [10,18].

Samples, which were post-incubated for an additional 24 h after exposure for 10 and 30 min, contained 1.2 (SD 0.0, $n = 3$) and 6.7 (SD 0.3, $n = 4$) μg respectively. This was over 80% of total deposited Ce mass.

To assess the analytic quality of CeO_2 detection by the use of ICP-MS, a cerium mass balance was calculated (Fig. S3). The cerium content of the washing waste of representative samples washed either immediately after 30 min particle exposure or after an additional 24 h incubation was determined to be 1.7 μg (SD 1.4, $n = 2$) and 0.4 μg (SD 0.1, $n = 3$), respectively. Together with the mean internalized cerium in the corresponding wells (4.6 μg (SD 1.4) and 6.7 μg (SD 0.3)), approximately 85% of the total deposited CeO_2 could be recovered.

3.5. Control experiments

Cells exposed for 30 min to particle-free flame off-gasses served as an internal control (baseline) and cultures placed separately in an incubator during the experiment served as external controls. Regarding culture confluence and overall cellular morphology, no differences compared to the internal control could be observed by the analysis of randomly selected transmission electron micrographs (data not shown). Furthermore, the integrity of the biological material was demonstrated under exposure conditions by excluding cellular lactate dehydrogenase (LDH) release. The baseline appeared unaffected by the experimental conditions, as illustrated by the comparable gas (internal) – and external control (Fig. S4). These findings are in line with recently published data, obtained with the same experimental setup [22].

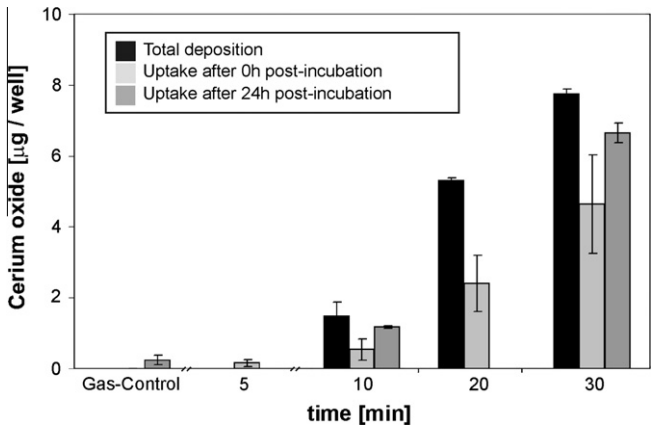

Fig. 3. Cerium oxide uptake kinetics. Cerium oxide total deposition on and internalization in A549 monocultures (internal dose) were quantified by inductively coupled plasma mass spectrometry (ICP-MS). Over 35% of the total deposited cerium mass could be found intracellularly after 10 min particle exposure, a value increasing to 60% after 30 min exposure. Following additional 24 h post-incubation, a time span after which adverse biological effects were observed in a previous experiment, approx. 80% of total mass was found to be cell associated after the washing procedure.

3.6. Verification of washing procedure

As the discrimination between surface deposited and intracellular cerium is a crucial point in this study, the efficiency of the applied washing procedure had to be assessed. Extracellular cerium was thought to be immersed in the aqueous lining layer and to decorate the A549 apical plasma membrane. It was assumed that the removal of this adherent CeO_2 fraction by washing goes along with the removal of these two extracellular structures. A considerable reduction of surfactant and hypophase could be demonstrated in control cell cultures, cultivated for 1 day at the air–liquid interface, illustrating the efficiency of the applied washing protocol (Fig. S5A).

Furthermore, no significant loss of cell material due to the washing procedure was found (Fig. S5B). Control cell cultures contained 3.3×10^6 (SD 3.7×10^5) cells/well after 1 day ($n = 3$) air–liquid exposure and 3.1×10^6 (SD 7.2×10^5) cells/well after 2 days ($n = 3$). Following the washing step, the cell number decreased slightly to 3.0×10^6 (SD 3.3×10^5) and 2.9×10^6 (SD 7.2×10^5) in one and two day air-exposed cultures, respectively.

4. Discussion

The aim of this study was to investigate the uptake kinetics of a representative nanoparticle into air–liquid cultivated A549 epithelial cell cultures. The exposure system used was based on a passive and reproducible mass deposition. In a constantly mixed volume, primary particles and aggregates tend to agglomerate by collision causing the observed logarithmic decay of aerosolized particle mass by sedimentation forces.

In line with the literature [22], the deposited mass caused no necrosis of the A549 cultures, as no LDH release was observed. Furthermore, also no dose-dependent morphological alterations were noticed at these comparable high-exposure concentrations.

The cerium deposition increased over the investigated time span, which was found to be in good agreement with the observed simultaneous decrease in aerosol mass concentration. The formation of agglomerates and their size-gain over time favoured an efficient mass deposition mainly by gravitational sedimentation. This behaviour was demonstrated in a cell-free environment by analyzing the cumulative mass deposition onto TEM grids, which were placed inside a cell culture plate and exposed to the cerium aerosol over different time spans. Mainly aggregates of various sizes, increasing in diameter over time, were found, but almost no single particles were detectable.

As under cell-free conditions, such focal cerium aggregates were also observed decorating the apical surface of exposed A549 cell cultures. Comparable surface-associated protrusions, thought to be composed of nanoparticles, have been described in another cell model after exposure to a CeO_2 suspension [54]. Furthermore, analogous aggregates were also found on the lung surface of animals of an inhalation study with titanium dioxide, illustrating the comparability of the applied deposition mode with

in vivo data [54]. Additionally, cerium oxide was also found inside A549 cells. It was mainly found to be aggregated in vesicles, which was previously reported in the literature for immersed exposure conditions [21,39].

We propose agglomeration as the key factor controlling the deposition of nanoparticles onto air-exposed cell cultures out of an atmosphere, containing a relative high particle burden. Based on this finding, which is in good agreement to earlier studies on suspended particles [51], the often propagated exposure of biological systems to monodisperse, singe-particle aerosols is of limited relevance and does not reflect conditions in occupational and environmental scenarios.

A substantial amount of the total deposited cerium oxide was found to be internalized almost immediately. Within an additional 24 h post-incubation, the cellular CeO_2 content increased further to approximately 80% of the deposited mass. The conclusion that most deposited particles are readily taken up by the cells, is in line with observations of CeO_2 suspensions with identical physicochemical properties, studied previously by Limbach et al. [21]. The authors quantified the internalization of flame-made cerium oxide NPs at low, physiological relevant suspension concentrations by human fibroblast monocultures with ICP-MS and provided a mathematical interpretation of the therewith obtained kinetic data. The resulting model identified particle mass transport processes, diffusion and sedimentation, as the rate-limiting factors for particle uptake compared to the biological membrane-trafficking processes. The consistency in short-term cerium uptake kinetics, independent of the exposure strategy (suspension or aerosol), makes the argumentations from the model by Limbach et al. also applicable to aerosol exposure scenarios. We propose a transport limitation of particle uptake by cells for aerosol and in suspension exposure scenarios.

In nanotoxicology, a majority of current *in vitro* approaches are based on the exposure of particles in a suspended state, a methodology originating in the classical toxicity testing of chemical compounds [55]. Great efforts were made towards more realistic exposure protocols, especially in pulmonary toxicology. The advent of *in vitro* aerosol exposure systems in lung toxicology raised a controversial scientific discussion on the comparability of toxicological data with such obtained from classical suspension exposure scenarios. From the physicochemical point of view, particle dispersions in liquid (suspensions) and such in gas (aerosols) behave according to the same principals. Additionally in both aerosol and in suspension, the uptake of particles by cells is transport limited. This paradigm also holds true for uptake kinetics, as demonstrated experimentally with this study. It can be concluded that current toxicological approaches, based on exposure to particle suspensions, might be considered more realistic and valid as one would expect from the known limitations of this exposure scenario (as example dosage) [53]. This also appreciates the already existing broad body of literature on NP toxicology, generated mainly under submerged conditions.

However, it has to be considered that under submerged conditions a variety of inherent parameters of the used dispersion medium, such as the cell culture's protein content, ionic strength and pH, might modify particle agglomeration and deposition behaviour in an uncontrollable and unrealistic manner. The exclusion of such alterations is a major advantage of aerosol exposure besides the more realistic and controllable dosage.

The fundamental understanding of mechanisms and limitations of NP uptake by biological systems is crucial for assessing their possible adverse health potential. Therefore, uptake kinetics and the underlying limiting factors of particle internalization have to be investigated for further particle types and more prolonged time spans in future research. However, the here reported already available data, which point towards comparable uptake kinetics of aerosolized and suspended cerium oxide NPs, are of great importance for the interpretation and future planning of toxicity screening studies.

Acknowledgments

The authors would like to thank Andrea Stokes and Mohammed Ouanella for the excellent technical assistance in preparing samples for electron microscopy. This work was financially supported by the Lung league Bern, by the Swiss Nanoscience Institute (SNI) within the National Center of Research (NCCR) in Nanoscale Science and the German Research Foundation (DFG SPP 1313).

Appendix A. Supplementary material

Supplementary data associated with this article can be found, in the online version, at doi:10.1016/j.ejpb.2010.11.017.

References

[1] H.K. Kammler, L. Madler, S.E. Pratsinis, Flame synthesis of nanoparticles, Chem. Eng. Technol. 24 (2001) 583–596.
[2] W.J. Stark, S.E. Pratsinis, Aerosol flame reactors for manufacture of nanoparticles, Powder Technol. 126 (2002) 103–108.
[3] K. Wegner, S.E. Pratsinis, Scale-up of nanoparticle synthesis in diffusion flame reactors, Chem. Eng. Sci. 58 (2003) 4581–4589.
[4] R.J. Aitken, K.S. Creely, C.L. Tran, Nanoparticles: an occupational hygiene review, Health Safety Executive Res. Report 274 (2004).
[5] A. Nel, T. Xia, L. Madler, N. Li, Toxic potential of materials at the nanolevel, Science 311 (2006) 622–627.
[6] A.P. Alberola, J.O. Radler, The defined presentation of nanoparticles to cells and their surface controlled uptake, Biomaterials 30 (2009) 3766–3770.
[7] I. Stayton, J. Winiarz, K. Shannon, Y.F. Ma, Study of uptake and loss of silica nanoparticles in living human lung epithelial cells at single cell level, Anal. Bioanal. Chem. 394 (2009) 1595–1608.
[8] M.R. Lorenz, V. Holzapfel, A. Musyanovych, K. Nothelfer, P. Walther, H. Frank, K. Landfester, H. Schrezenmeier, V. Mailander, Uptake of functionalized fluorescent-labeled polymeric particles in different cell lines and stem cells, Biomaterials 27 (2006) 2820–2828.
[9] M.R. Lorenz, M.V. Kohnle, M. Dass, P. Walther, A. Hocherl, U. Ziener, K. Landfester, V. Mailander, Synthesis of fluorescent polyisoprene nanoparticles and their uptake into various cells, Macromol. Biosci. 8 (2008) 711–727.
[10] J. DavdaV. Labhasetwar, Characterization of nanoparticle uptake by endothelial cells, Int. J. Pharm. 233 (2002) 51–59.
[11] M.P. Desai, V. Labhasetwar, E. Walter, R.J. Levy, G.L. Amidon, The mechanism of uptake of biodegradable microparticles in Caco-2 cells is size dependent, Pharm. Res. 14 (1997) 1568–1573.
[12] M.G. Qaddoumi, H. Ueda, J. Yang, J. Davda, V. Labhasetwar, V.H.L. Lee, The characteristics and mechanisms of uptake of PLGA nanoparticles in rabbit conjunctival epithelial cell layers, Pharm. Res. 21 (2004) 641–648.
[13] B.D. Chithrani, A.A. Ghazani, W.C.W. Chan, Determining the size and shape dependence of gold nanoparticle uptake into mammalian cells, Nano Lett. 6 (2006) 662–668.
[14] B.D. Chithrani, W.C.W. Chan, Elucidating the mechanism of cellular uptake and removal of protein-coated gold nanoparticles of different sizes and shapes, Nano Lett. 7 (2007) 1542–1550.
[15] E.C. Cho, J.W. Xie, P.A. Wurm, Y.N. Xia, Understanding the role of surface charges in cellular adsorption versus internalization by selectively removing gold nanoparticles on the cell surface with a I-2/KI Etchant, Nano Lett. 9 (2009) 1080–1084.
[16] C. Bandenberger, C. Muhlfeld, Z. Ali, A.G. Lenz, O. Schmid, W.J. Parak, P. Gehr, B. Rothen-Rutishauser, Quantitative evaluation of cellular uptake and trafficking of plain and polyethylene glycol-coated gold nanoparticles, Small 6 (2010).
[17] H. Jin, D.A. Heller, R. Sharma, M.S. Strano, Size-dependent cellular uptake and expulsion of single-walled carbon nanotubes: single particle tracking and a generic uptake model for nanoparticles, ACS Nano 3 (2009) 149–158.
[18] L.Y. Zha, Z.R. Xu, M.Q. Wang, L.Y. Gu, Chromium nanoparticle exhibits higher absorption efficiency than chromium picolinate and chromium chloride in Caco-2 cell monolayers, J. Anim. Physiol. Anim. Nutr. 92 (2008) 131–140.
[19] C. Wilhelm, F. Gazeau, J. Roger, J.N. Pons, J.C. Bacri, Interaction of anionic superparamagnetic nanoparticles with cells: kinetic analyses of membrane adsorption and subsequent internalization, Langmuir 18 (2002) 8148–8155.
[20] C. Wilhelm, C. Billotey, J. Roger, J.N. Pons, J.C. Bacri, F. Gazeau, Intracellular uptake of anionic superparamagnetic nanoparticles as a function of their surface coating, Biomaterials 24 (2003) 1001–1011.
[21] L.K. Limbach, Y.C. Li, R.N. Grass, T.J. Brunner, M.A. Hintermann, M. Muller, D. Gunther, W.J. Stark, Oxide nanoparticle uptake in human lung fibroblasts: effects of particle size, agglomeration, and diffusion at low concentrations, Environ. Sci. Technol. 39 (2005) 9370–9376.

[22] B. Rothen-Rutishauser, R.N. Grass, F. Blank, L.K. Limbach, C. Muehlfeld, C. Brandenberger, D.O. Raemy, P. Gehr, W.J. Stark, Direct combination of nanoparticle fabrication and exposure to lung cell cultures in a closed setup as a method to simulate accidental nanoparticle exposure of humans, Environ. Sci. Technol. 43 (2009) 2634–2640.
[23] J. Seagrave, S. Dunaway, J.D. McDonald, J.L. Mauderly, P. Hayden, C. Stidley, Responses of differentiated primary human lung epithelial cells to exposure to diesel exhaust at an air–liquid interface, Exp. Lung Res. 33 (2007) 27–51.
[24] S. Abe, H. Takizawa, I. Sugawara, S. Kudoh, Diesel exhaust (DE)-induced cytokine expression in human bronchial epithelial cells – a study with a new cell exposure system to freshly generated DE in vitro, Am. J. Respir. Cell Mol. Biol. 22 (2000) 296–303.
[25] A.L. Holder, D. Lucas, R. Goth-Goldstein, C.P. Koshland, Cellular response to diesel exhaust particles strongly depends on the exposure method, Toxicol. Sci. 103 (2008) 108–115.
[26] M. Geiser, S. Schurch, P. Gehr, Influence of surface chemistry and topography of particles on their immersion into the lung's surface-lining layer, J. Appl. Physiol. 94 (2003) 1793–1801.
[27] J. Gil, E.R. Weibel, Extracellular lining of bronchioles after perfusion-fixation of rat lungs for electron microscopy, Anat. Rec. 169 (1971) 185.
[28] P. Gehr, M. Geiser, V.I. Hof, S. Schuerch, L.M. Cruzorive, Stereological estimation of particle retention and clearance in the intrapulmonary conducting airways of the hamster lungs, J. Aerosol Sci. 21 (1990) 362.
[29] S. Schurch, P. Gehr, V.I. Hof, M. Geiser, F. Green, Surfactant displaces particles toward the epithelium in airways and alveoli, Respir. Physiol. 80 (1990) 17–32.
[30] S. Schurch, M. Geiser, M.M. Lee, P. Gehr, Particles at the airway interfaces of the lung, Colloids Surf., B 15 (1999) 339–353.
[31] B.T. Kilbourn, Cerium and cerium compounds, in: A. Seidel (Ed.), Kirk–Othmer Encyclopedia of Chemical Technology, fifth ed., vol. 5, Wiley Interscience, Hoboken, NJ, 2004, pp. 670–692.
[32] K. Reinhardt, H. Winkler, Cerium mischmetal, cerium alloys, and cerium compounds, in: A. Seidel (Ed.), Illmann's Encyclopedia of Industrial Chemistry, sixth ed., vol. 7, Wiley-VCH Verlag GmbH & Co. KGaA, Weinheim, Germany, 2003, pp. 285–300.
[33] M. G. Costantini, Evaluation of Human Health Risk from Cerium Added to Diesel Fuel, Health Effects Institute, Communication 9, 2001.
[34] M. Fall, M. Guerbet, B. Park, F. Gouriou, F. Dionnet, J.P. Morin, Evaluation of cerium oxide and cerium oxide based fuel additive safety on organotypic cultures of lung slices, Nanotoxicology 1 (2007) 227–234.
[35] B. Park, P. Martin, C. Harris, R. Guest, A. Whittingham, P. Jenkinson, J. Handley, Initial in vitro screening approach to investigate the potential health and environmental hazards of Envirox™ – a nanoparticulate cerium oxide diesel fuel additive, Part. Fibre Toxicol. 4 (2007).
[36] B. Park, K. Donaldson, R. Duffin, L. Tran, F. Kelly, I. Mudway, J.P. Morin, R. Guest, P. Jenkinson, Z. Samaras, M. Giannouli, H. Kouridis, P. Martin, Hazard and risk assessment of a nanoparticulate cerium oxide-based diesel fuel additive – a case study, Inhal. Toxicol. 20 (2008) 547–566.
[37] K. Van Hoecke, J.T.K. Quik, J. Mankiewicz-Boczek, K.A.C. De Schamphelaere, A. Elsaesser, P. Van der Meeren, C. Barnes, G. McKerr, C.V. Howard, D. Van De Meent, K. Rydzynski, K.A. Dawson, A. Salvati, A. Lesniak, I. Lynch, G. Silversmit, B. De Samber, L. Vincze, C.R. Janssen, Fate and effects of CeO_2 nanoparticles in aquatic ecotoxicity tests, Environ. Sci. Technol. 43 (2009) 4537–4546.
[38] H.J. Eom, J. Choi, Oxidative stress of CeO_2 nanoparticles via p38-Nrf-2 signaling pathway in human bronchial epithelial cell Beas-2B, Toxicol. Lett. 187 (2009) 77–83.
[39] T. Xia, M. Kovochich, M. Liong, L. Madler, B. Gilbert, H.B. Shi, J.I. Yeh, J.I. Zink, A.E. Nel, Comparison of the mechanism of toxicity of zinc oxide and cerium oxide nanoparticles based on dissolution and oxidative stress properties, ACS Nano 2 (2008) 2121–2134.
[40] L. Kappenberger, A.A. Bühlmann, Lungenveränderungen durch "Seltene Erden", Swiss Med. Wkly. 105 (1975).
[41] J.W. Mcdonald, A.J. Ghio, C.E. Sheehan, P.F. Bernhardt, V.L. Roggli, Rare-earth (cerium oxide) pneumoconiosis – analytical scanning electron-microscopy and literature-review, Mod. Pathol. 8 (1995) 859–865.
[42] J.C. Pairon, F. Roos, Y. Iwatsubo, X. Janson, M.A. Billongalland, J. Bignon, P. Brochard, Lung retention of cerium in humans, Occup. Environ. Med. 51 (1994) 195–199.
[43] J.C. Pairon, F. Roos, P. Sebastien, B. Chamak, I. Abdalsamad, J.F. Bernaudin, J. Bignon, P. Brochard, Biopersistence of cerium in the human respiratory-tract and ultrastructural findings, Am. J. Ind. Med. 27 (1995) 349–358.
[44] P. Vogt, M.A. Spycher, J.R. Rüttner, Pneumokoniose durch "Seltene erden" (Cer-Pneumokoniose), Schweiz. med. Wschr. 116 (1986) 1303–1308.
[45] S. Patil, A. Sandberg, E. Heckert, W. Self, S. Seal, Protein adsorption and cellular uptake of cerium oxide nanoparticles as a function of zeta potential, Biomaterials 28 (2007) 4600–4607.
[46] B. Rothen-Rutishauser, F. Blank, C. Muhlfeld, P. Gehr, In vitro models of the human epithelial airway barrier to study the toxic potential of particulate matter, Expert Opin. Drug Metab. Toxicol. 4 (2008) 1075–1089.
[47] S. Loher, W.J. Stark, M. Maciejewski, A. Baiker, S.E. Pratsinis, D. Reichardt, F. Maspero, F. Krumeich, D. Gunther, Fluoro-apatite and calcium phosphate nanoparticles by flame synthesis, Chem. Mater. 17 (2005) 36–42.
[48] F. Blank, B.M. Rothen-Rutishauser, S. Schurch, P. Gehr, An optimized in vitro model of the respiratory tract wall to study particle cell interactions, J. Aerosol Med. 19 (2006) 392–405.
[49] C. Mühlfeld, B. Rothen-Rutishauser, D. Vanhecke, F. Blank, P. Gehr, M. Ochs, Visualization and quantitative analysis of nanoparticles in the respiratory tract by transmission electron microscopy, Part. Fibre Toxicol. 4 (2010).
[50] C. Bandenberger, M.J.D. Clift, D. Vanhecke, C. Muhlfeld, V. Stone, P. Gehr, B. Rothen-Rutishauser, Intracellular imaging of nanoparticles: is it an elemental mistake to believe what you see? Part. Fibre Toxicol. 7 (2010).
[51] T.J. Brunner, P. Wick, P. Manser, P. Spohn, R.N. Grass, L.K. Limbach, A. Bruinink, W.J. Stark, In vitro cytotoxicity of oxide nanoparticles: comparison to asbestos, silica, and the effect of particle solubility, Environ. Sci. Technol. 40 (2006) 4374–4381.
[52] K.W. Powers, S.C. Brown, V.B. Krishna, S.C. Wasdo, B.M. Moudgil, S.M. Roberts, Research strategies for safety evaluation of nanomaterials. Part VI. Characterization of nanoscale particles for toxicological evaluation, Toxicol. Sci. 90 (2006) 296–303.
[53] J.G. Teeguarden, P.M. Hinderliter, G. Orr, B.D. Thrall, J.G. Pounds, Particokinetics in vitro: dosimetry considerations for in vitro nanoparticle toxicity assessments, Toxicol. Sci. 95 (2007) 300–312.
[54] J. Schnekenburger, R. Landsiedel, M. Wiemann, S. Brill, J. Bruch, D. Geiger, D. Hahn, A. Kroll, H. F. Krug, C.-M. Lehr, L. Ma-Hock, S. Mülhopt, K. Nau, J. Pauluhn, H.-R. Paur, M.H. Pillukat, J. Tagot, U.F. Schäfer, C. Schulze, K. Tönsing, D. Wesner, K. Wiench, W. Wohlleben, S. Zünkeler, Toxicological Studies, in: T.A.J. Kuhlbusch, H.F. Krug, K. Nau (Eds.), NanoCare Health related Aspects of Nanomaterials, Final Scientific Report, Dechema e.V., Frankfurt am Mein, Germany, 2009, pp. 22–73.
[55] L.K. Limbach, R.N. Grass, W.J. Stark, Physico-chemical differences between particle- and molecule-derived toxicity: can we make inherently safe nanoparticles?, Chimia 63 (2009) 38–43